

Various Examples of the Types of Measurement Capabilities on BT7

Jeffrey Lynn
NIST Center for Neutron Research

OBJECTIVES: We provide a few examples, with brief explanations, of some of the types of measurements that can be carried out on BT-7.

I. Powder Diffraction Using the PSD

The PSD can be used with a radial collimator and no energy analyzer to obtain a powder diffraction pattern. One of the first measurements of this type was carried out on LaFeAsO, the parent material of the iron-based high T_C superconductors [1]. This is a coarse resolution-high intensity configuration to search for weak magnetic peaks. The strong peaks in Fig. 1 (top) are the structural peaks, while at low temperatures you can just see the very weak magnetic

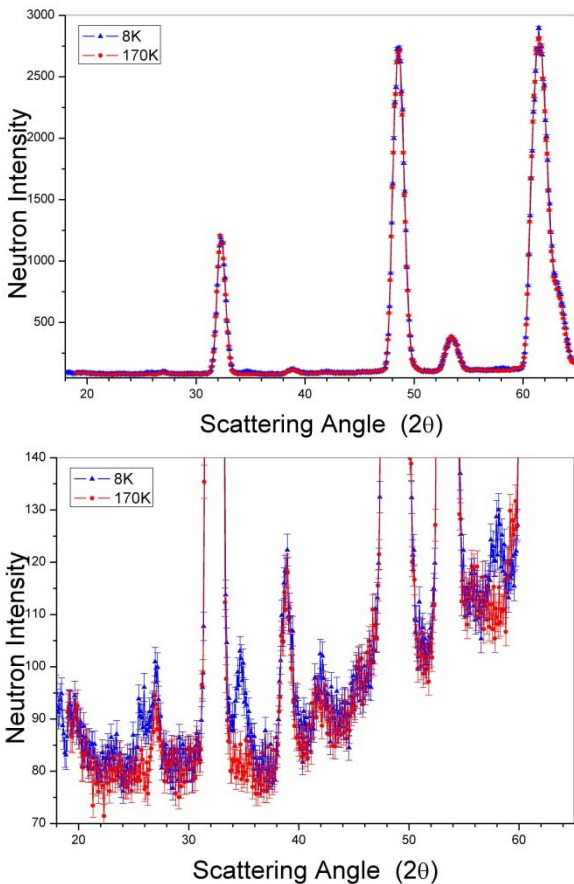


Fig. 1. (a) Powder diffraction pattern for LaFeAsO above (170 K) and below (8 K) the antiferromagnetic phase transition.[1]

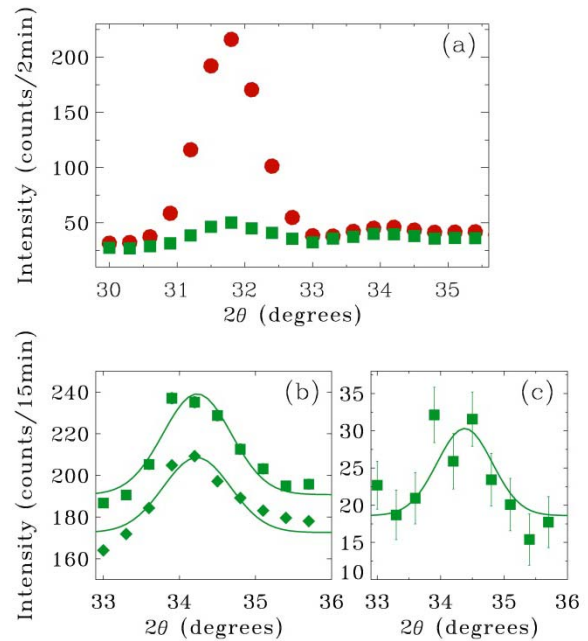


Fig. 2. (a) Non-spin-flip (red) and spin-flip (green) scattering for the structural Bragg peak. (b) Spin-flip scattering with $\mathbf{P} \parallel \mathbf{Q}$ and $\mathbf{P} \perp \mathbf{Q}$, and (c) their subtraction. Only magnetic scattering can flip the neutron spin.[2]

peaks appear. These peaks are clearly seen in the expanded scale (Fig.1 bottom) at about 26, 34, and 59 degrees scattering angle.

Polarized beam techniques can be employed to determine unambiguously that these small new peaks are magnetic in origin. Fig. 2 (top) shows the non-spin-flip (red) and spin-flip (green) scattering for the structural Bragg peak of NdFeAsO; the weak spin-flip scattering is just due to the finite polarization of the instrument; ideally it would be identically zero. For the magnetic peak (bottom) we find only spin-flip (magnetic) scattering. Note that substantial intensity is lost due to polarizing the incident beam and then analyzing the polarization. Hence most often the polarized beam technique is used to uniquely identify magnetic or structural scattering, and only needs to be carried out once.

The intensity of the magnetic peak is directly proportional to the square of the ordered magnetic moment—the order parameter of the phase transition. Fig. 3 (top) shows the integrated intensity of the iron antiferromagnetic peak vs. T , which indicates a phase transition at 133 K. This was a surprise as the tetragonal—orthorhombic structural transition occurs much higher, at 155 K. Fig. 3(bottom) shows the order parameter for the Nd ordering in NdFeAsO [3].

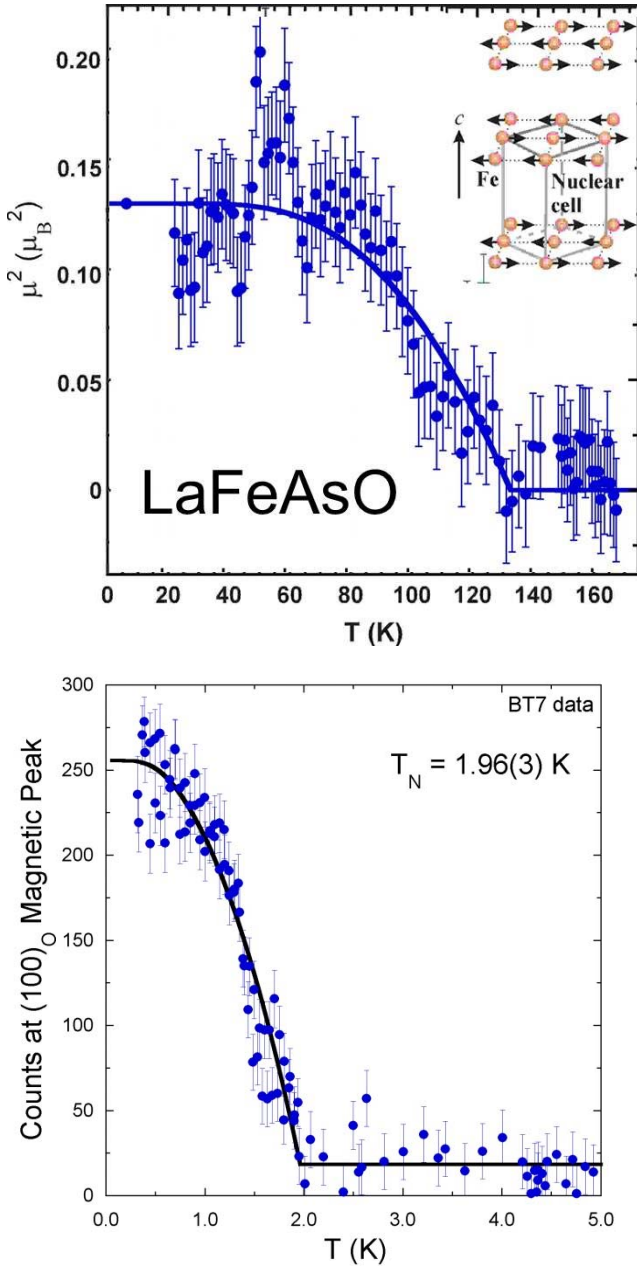


Fig.3 (top) Fe order parameter for LaFeAsO [1]. (bottom) Nd order parameter for NdFeAsO [3].

II. Single Crystal Diffraction with the PSD

Fig. 4 shows a map of the $(H, K, 0)$ scattering plane for Co_3TeO_6 , which exhibits both magnetic and ferroelectric properties [4]. The initial magnetic ordering develops below 26 K, where four incommensurate magnetic satellite peaks surround the fundamental structural Bragg peaks at integer positions. Note that the ordering wave vector is incommensurate in both H and K . At 19.5 K commensurate magnetic peaks develop in addition to the incommensurate satellite peaks. Thus there are both structural and magnetic components of the scattering at the integer positions. At 18 K both the commensurate and incommensurate structures change, and ferroelectricity develops. At 16 K the final changes in the magnetic structures occur and ferroelectricity is lost. The map in Fig. 4 shows the scattering in the ground state, which exhibits both incommensurate satellite peaks and fundamental magnetic and structural peaks at the integer positions.

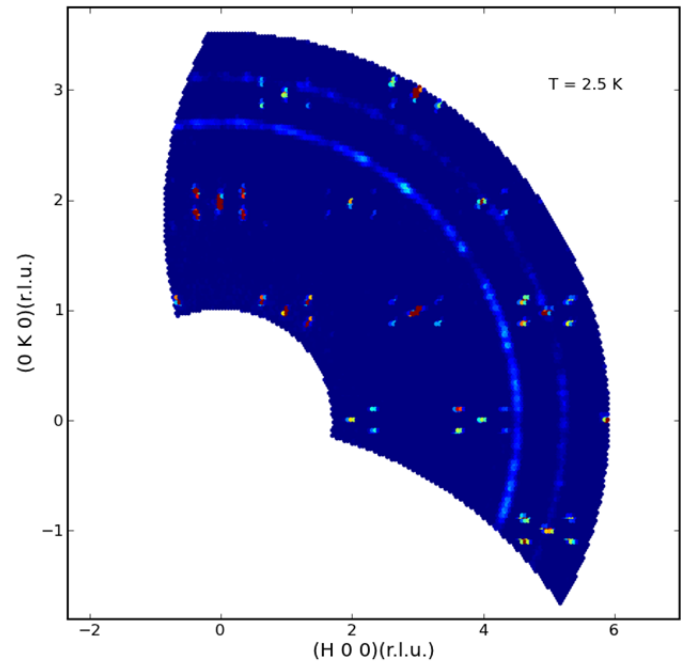


Fig. 4 Map of the $(H, K, 0)$ scattering plane in the multiferroic Co_3TeO_6 , showing the incommensurate satellite peaks surrounding the fundamental peaks. These commensurate peaks have both structural and magnetic contributions. The ring of scattering is the $\{111\}$ powder line from the Al holder. Note that it is not uniform in intensity, but shows considerable preferred orientation, as is of the case for machined parts.[4]

III. Polarized Beam Single Crystal Diffraction

$\text{Ni}_3\text{V}_2\text{O}_8$ (NVO) is an insulating multiferroic magnet with spin-1 Ni^{2+} ions arranged in a buckled kagome-staircase geometry. When the ferroelectric and magnetic phases coexist and the spin and charge are strongly coupled, there is the possibility of controlling magnetic properties through an electric field E , and such a nonlinear magnetoelectric response is both of fundamental interest and holds the potential for applications that include sensing, spintronics, and microwave communication.

NVO first forms an incommensurate magnetic structure just above 9 K, and then develops an incommensurate spiral phase below 6.4 K which is accompanied by ferroelectricity. The domains of this cycloidal magnetic structure can be controlled by an applied E . Fig. 5 shows the polarized magnetic diffraction cross section. The handedness of the spiral can be controlled, first by cooling in an applied electric field of +300 V, and then by cooling in a field of -300 V. The handedness can be unambiguously determined using polarized neutron scattering as shown in the figure [5].

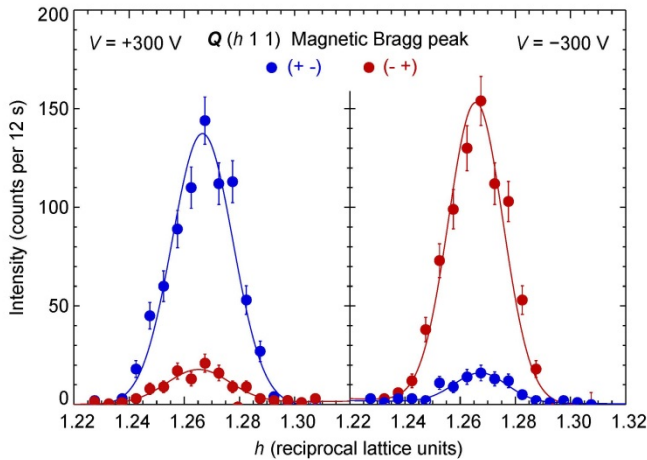


Fig. 5. Polarized magnetic diffraction in an electric field under opposite spin-flip scattering conditions. Statistical uncertainties represent 1 standard deviation. (a) Cooling in a field $E = +300$ kV/m from 11 to 5 K (E-cooling) favors cycloidal domains that predominantly diffract neutrons polarized antiparallel to Q . (b) Reversing E yields the opposite polarized intensity asymmetry.[5]

IV. Inelastic Magnetic Scattering

The dynamics of materials are investigated via inelastic scattering, and generally we employ the technique of having a fixed final energy on the instrument (for example $E_f = 14.7$ meV) and vary the incident energy, with $E_i > E_f$ so that the neutrons destroy an elementary excitation in the system and lose energy. The excitations of interest can be magnons, phonons, excitons, or crystal field levels for example, or fluctuations in the disordered state.

Generally it is preferable to have a single crystal sample where the dispersion relations can be mapped in different directions, but if suitable single crystals are not available then useful information still can be obtained on polycrystalline samples. An example of the latter concerns the magnetic ordering and magnon excitations in $\text{Ba}_{0.56}\text{Sr}_{0.44}\text{MnO}_3$. [6] This material becomes ferroelectric above room

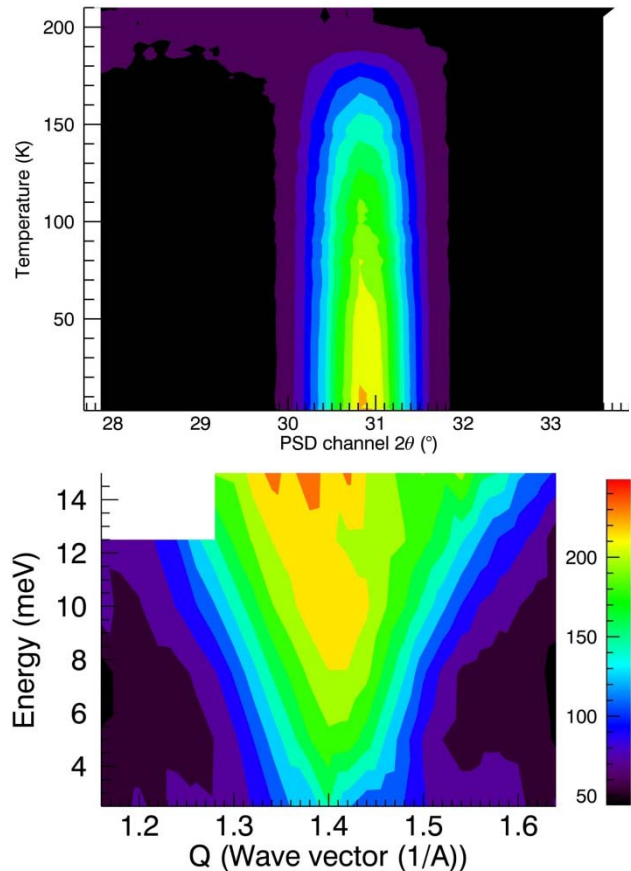


Fig. 6. (top) Intensity vs. temperature for the magnetic Bragg peak. (Bottom) Inelastic magnetic scattering measured vs. energy transfer at low T (2.5 K), which determines the magnon density-of-states.[6]

temperature, and orders antiferromagnetically at 200 K as shown in Fig. 6. These data are obtained using the PSD at a single angular setting of the instrument and simply varying the temperature. The inelastic scattering is shown in Fig. 6 (bottom), and were taken using the analyzer system in horizontal energy focusing mode. The ground state spin dynamics is characterized by a spin gap of 4.6(5) meV and the magnon density of states peaks at 43 meV. Detailed spin wave simulations with a gap and isotropic exchange of $J = 4.8(2)$ meV describe the excitation spectrum well. Above T_N strong spin correlations coexist with robust ferroelectric order.

Much more detailed information can be obtained on a single crystal sample, as the magnon dispersion relations can be measured directly rather than just the magnon density-of-

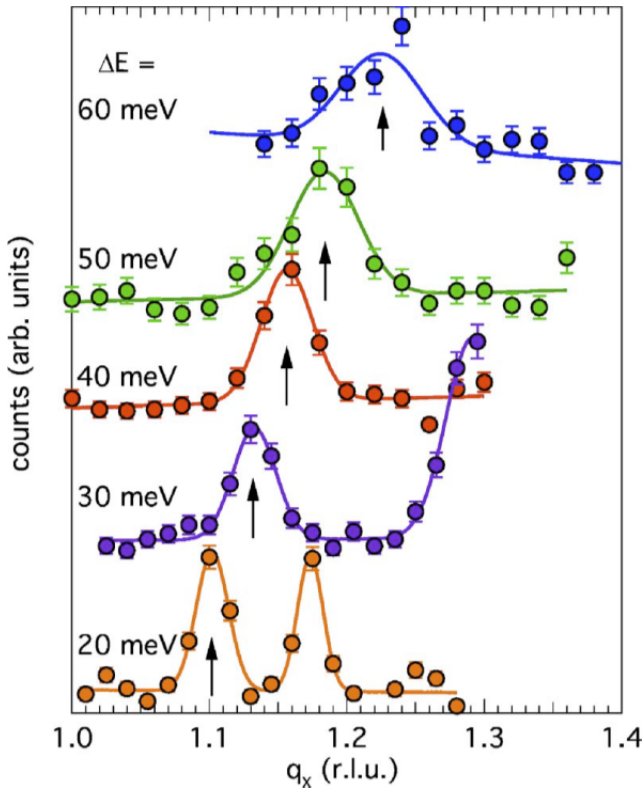


Fig. 7. Constant energy transfer scans for the $\text{Fe}_{0.835}\text{Ga}_{0.165}$ magnetoelastic system, showing the dispersion of the magnons to larger wave vectors as the energy is increased. For the scans at 20 and 30 meV the peaks on the right hand side of the scans are the longitudinal acoustic phonon mode.[7]

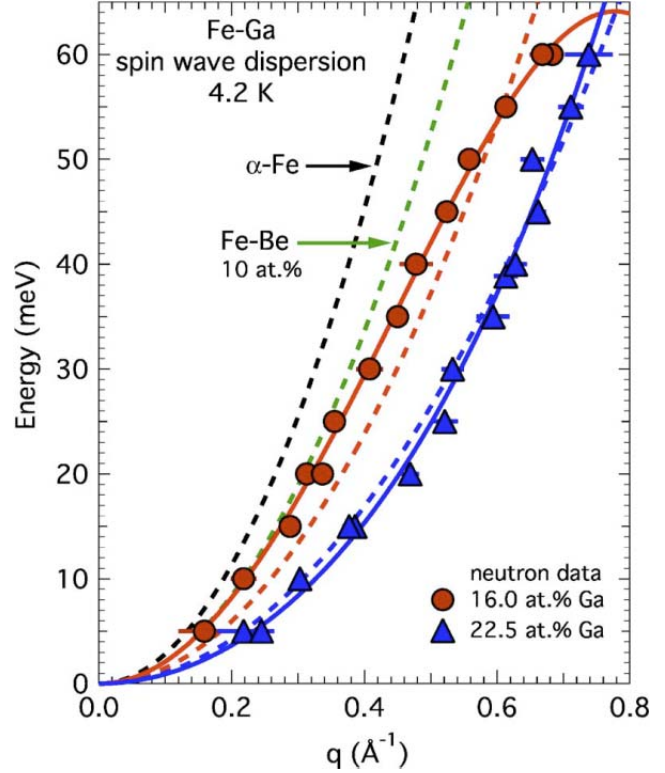


Fig. 8. Ground state magnon dispersion relations for two $\text{Fe}_{1-x}\text{Ga}_x$ alloys, $x=0.108$ (red circles) and $x=0.225$ (blue triangles). The dashed curves, in order of decreasing D , are quadratic fits for Fe (black), $\text{Fe}_{1-x}\text{Be}_x$, ($x=0.10$ green), and $\text{Fe}_{1-x}\text{Ga}_x$, $x=0.160$ (red) and $x=0.225$ (blue). The solid curves are quadratic and fourth-order fits for the two Fe-Ga alloys.[7]

states. Figures 7 and 8 show the data for magnons (and a few phonons) in the magnetoelastic material $\text{Fe}_{0.835}\text{Ga}_{0.165}$. [7] Generally gram-size single crystals are required for such measurements.

Polarized Inelastic Scattering

Since neutrons scatter coherently from both the nuclei (structural scattering) and the electron's magnetism (magnetic scattering), there can be ambiguity in identifying a measured cross section. Nuclear coherent scattering (structural Bragg peaks, phonons) never causes a reversal, or spin-flip, of the neutron. Thus, the nuclear peaks will only be observed in the non-spin-flip scattering geometry. The magnetic cross-sections, on the other hand, depend on the

relative orientation of the neutron polarization \mathbf{P} and the scattering vector \mathbf{Q} . In the configuration where $\mathbf{P} \perp \mathbf{Q}$ typically half the magnetic Bragg scattering involves a reversal of the neutron spin and half does not, while for $\mathbf{P} \parallel \mathbf{Q}$ all the magnetic scattering is spin-flip. Hence, for a pure magnetic Bragg reflection the spin-flip scattering should be twice as strong for the $\mathbf{P} \parallel \mathbf{Q}$ configuration, and subtraction of the $\mathbf{P} \perp \mathbf{Q}$ scattering from the $\mathbf{P} \parallel \mathbf{Q}$ scattering yields an unambiguous magnetic signal as shown in Fig. 2(c).

For inelastic scattering only magnetic scattering is spin-flip and is maximal for $\mathbf{P} \parallel \mathbf{Q}$ as shown in Fig. 9.[8] This is a measurement of the spin-flip scattering intensity, varying \mathbf{Q} at a constant energy transfer of 34 meV, through the ‘magnetic resonance’ of this high temperature superconductor. The data directly demonstrate that this scattering is magnetic in origin.

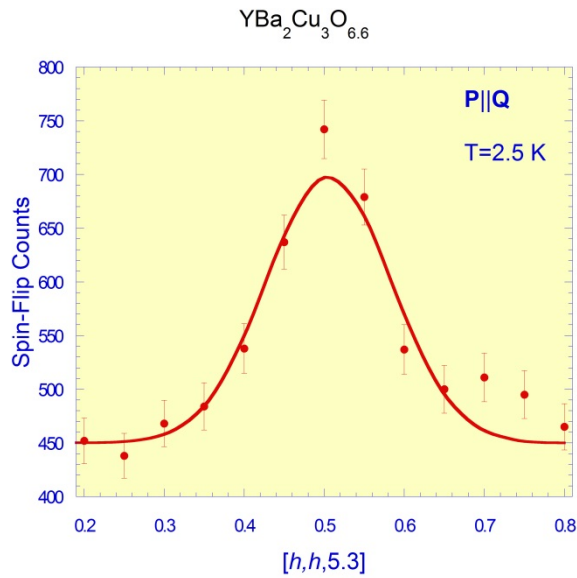


Fig. 9. Spin-flip scattering in the superconducting phase of $\text{YBa}_2\text{Cu}_3\text{O}_{6.6}$, at an energy transfer of 34 meV which corresponds to the resonant magnetic excitation.[8]

Lattice Dynamics

In addition to the magnon dispersion relations such as shown in Fig. 7, the phonon dispersion relations for single crystals can also be measured in a similar manner, and an example has already been mentioned in that figure. Figure 10 shows the phonon

dispersion relations along the $[0,1,0]$ direction for the relaxor ferroelectric PMN-30%PT $((\text{Pb}(\text{Mg}_{1/3}\text{Nb}_{2/3})\text{O}_3)70\%-(\text{PbTiO}_3)30\%)$ at high temperature. The transverse optical (TO) phonon branch and the transverse acoustic (TA) phonon branch are the conventional phonons modes in materials and are observed at all temperatures. Relaxor ferroelectrics have nanoscale polar distortions that give them their huge electromechanical response, and it turns out that these polar nanoregions are controlled by anharmonic effects that produce intrinsic localized modes in between these two branches.[9]

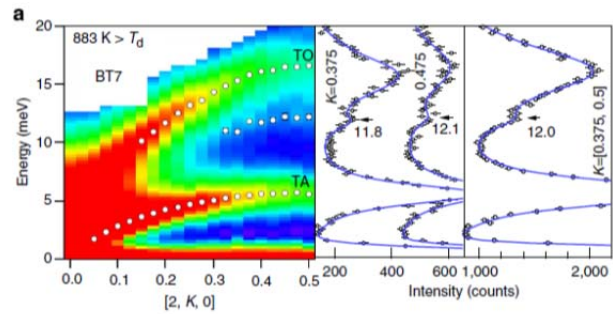


Fig. 10. On the left, spectrum measured along $\mathbf{Q}=[2, K, 0]$ at 883 K, which is a temperature well above the Burns temperature ($T_b=680$ K). The open circles indicate the peak positions from fits to the TA and TO modes and a much weaker localized mode in between. Panels on the right side show fits to the modes in the neutron spectrum at a few values of K , with data offset in intensity for clarity.[9]

The phonon data presented in Figs. 7 and 10 were taken using the ‘conventional’ triple technique, with horizontally flat monochromator and analyzer, and Söller collimators before and after both. This arrangement typically provides the best signal-to-noise, but the data are obtained one point at a time. An alternative technique is to use a radial collimator after the sample, flat analyzer and the PSD, as shown Fig. 11. The crystal is the colossal magnetoresistive oxide $\text{La}_{0.7}\text{Ca}_{0.3}\text{MnO}_3$, and the scattering being investigated is the lattice polaron scattering.[10] Here the instrument cuts through the polaron scattering for a single setting of the spectrometer. Two peaks in the lattice polaron dynamics are observed at $\pm q$ around the elastic (static) polaron peak position at $(0.25, 0.25, 0)$.

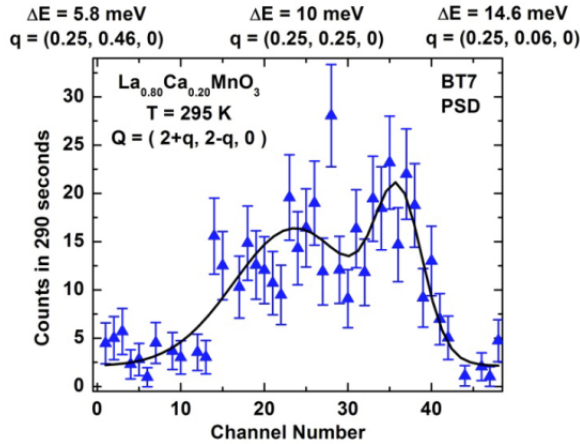


Fig. 11. Inelastic scattering measured on $\text{La}_{0.7}\text{Ca}_{0.3}\text{MnO}_3$ for a single setting of the spectrometer. For this mode the \mathbf{Q} and energy transfer are coupled together as shown on the top part of the x-axis.[10,11]

V. References

- [1] Magnetic Order Close to Superconductivity in the Iron-based Layered $\text{La}(\text{O}_{1-x}\text{F}_x)\text{FeAs}$ systems, C. de la Cruz, Q. Huang, J. W. Lynn, J. Li, W. Ratcliff II, J. L. Zarestky, H. A. Mook, G. F. Chen, J. L. Luo, N. L. Wang, and P. Dai, [Nature **453**, 899 \(2008\)](#).
- [2] Magnetic Order of the Iron Spins in NdOFeAs , Y. Chen, J. W. Lynn, J. Li, G. Li, G. F. Chen, J. L. Luo, N. L. Wang, Pengcheng Dai, C. dela Cruz, and H. A. Mook, [Phys. Rev. B **78**, 064515 \(2008\)](#).
- [3] Crystal Structure and Antiferromagnetic Order in $\text{NdFeAsO}_{1-x}\text{F}_x$ ($x = 0.0$ and 0.2): Superconducting Compounds from Neutron Diffraction Measurements, Y. Qiu, Wei Bao, Q. Huang, T. Yildirim, J. M. Simmons, M. A. Green, J.W. Lynn, Y. C. Gasparovic, J. Li, T. Wu, G. Wu, and X. H. Chen, [Phys. Rev. Lett. **101**, 257002 \(2008\)](#).
- [4] Interplay between the magnetic and electric degree-of-freedom in multiferroics Co_3TeO_6 , Wen-Hsien Li, Chin-Wei Wang, Daniel Hsu, Chi-Hung Lee, Chun-Ming Wu, Chih-Chieh Chou, Hung-Duen Yang, Yang Zhao, Sung Chang, Jeffrey W. Lynn, and Helmuth Berger, [Phys. Rev. B **85**, 094431 \(2012\)](#); Complex Magnetic Couplings in Co_3TeO_6 , Chin-Wei Wang, Chi-Hung Lee, Chi-Yen Li, Chun-Ming Wu, Wen-Hsien Li, Chih-Chieh Chou, Hung-Duen Yang, Jeffrey W. Lynn, Qingzhen Huang, A. Brooks Harris, and Helmuth Berger, [Phys. Rev. **B88**, 184427 \(2013\)](#).
- [5] Coupled Magnetic and Ferroelectric Domains in Multiferroic $\text{Ni}_3\text{V}_2\text{O}_8$, I. Cabrera, M. Kenzelmann, G. Lawes, Y. Chen, W. C. Chen, R. Erwin, T. R. Gentile, J. Leão, J. W. Lynn, N. Rogado, R. J. Cava, and C. Broholm, [Phys. Rev. Lett. **103**, 087201 \(2009\)](#).
- [6] Neutron Scattering Studies of Spin Dynamics in the Type-I Multiferroic $\text{Sr}_{0.56}\text{Ba}_{0.44}\text{MnO}_3$, D. K. Pratt, J. W. Lynn, J. Mais, O. Chmaissem, Dennis E. Brown, Stanislaw Kolesnik, and B. Dabrowski, [Phys. Rev. B **90**, 140401\(R\) \(2014\)](#).
- [7] Spin wave Dispersion in Magnetostrictive Fe-Ga alloys, J. L. Zarestky, O. Moze, J. W. Lynn, Y. Chen, T. A. Lograsso, and D. L. Schlager, [Phys. Rev. **B75**, 052406 \(2007\)](#).
- [8] M. B. Stone, J. W. Lynn, H. A. Mook, M. D. Lumsden, A. D. Christianson, and G. E. Granroth (private communication).
- [9] Phonon Localization Drives Polar Nanoregions in a Relaxor Ferroelectric, M. E. Manley, J. W. Lynn, E. D. Specht, O. Delaire, A. R. Bishop, R. Sahul, J. D. Budai, [Nature Commun. **5**, 3683 \(2014\)](#).
- [10] Order and Dynamics of Intrinsic Nanoscale Inhomogeneities in Manganites, J. W. Lynn, D. N. Argyriou, Y. Ren, Y. Chen, Y. M. Mukovskii, and D. A. Shulyatev, [Phys. Rev. B **76**, 014437 \(2007\)](#).
- [11] Double Focusing Thermal Triple Axis Spectrometer at the NCNR, J. W. Lynn, Y. Chen, S. Chang, Y. Zhao, S. Chi, W. Ratcliff, II, B. G. Ueland, and R. W. Erwin, [Journal of Research of NIST **117**, 61-79 \(2012\)](#).